

ALM-polynomial for Antiviral Drugs Targeting COVID-19 Treatment

Abhay Rajpoot^{1,*} 

¹ Department Of Mathematics, Indira Gandhi Govt. P G College, Bangarmau, Unnao, U. P., India

* Correspondence: abhayrajpoot.rs.mat17@itbhu.ac.in;

Received: 4.12.2023; Accepted: 12.05.2024; Published: 20.12.2025

Abstract: The global pandemic caused by the novel virus SARS-CoV-2, also known as COVID-19, has emerged as a critical public health crisis affecting populations worldwide. The lack of effective treatments has exacerbated the situation. In response to this ongoing pandemic, there is a concerted effort to investigate potential drugs for combating the disease. Topological indices, also known as molecular descriptors, are numerical parameters that relate a chemical compound's molecular structure to its physicochemical properties. These indices play a pivotal role in the development of QSPR/QSAR (quantitative structure-property relationship/quantitative structure-activity relationship) models, aiding in the search for effective solutions. In this study, we introduce the ALM-polynomial method to derive novel AL indices. Subsequently, we utilize this approach to compute AL indices for antiviral drugs, specifically Remdesivir (GS-5734), Chloroquine, Hydroxychloroquine, and Theaflavin. Additionally, the results of this analysis are visually presented in graphical form.

Keywords: topological indices; COVID-19; antiviral drug; QSPR analysis; 97M60; 05C35; 05C92; 62P10.

© 2025 by the authors. This article is an open-access article distributed under the terms and conditions of the Creative Commons Attribution (CC BY) license (<https://creativecommons.org/licenses/by/4.0/>), which permits unrestricted use, distribution, and reproduction in any medium, provided the original work is properly cited. The authors retain copyright of their work, and no permission is required from the authors or the publisher to reuse or distribute this article, as long as proper attribution is given to the original source.

1. Introduction

The virus responsible for causing the infectious disease known as coronavirus disease 2019 (COVID-19) is Severe Acute Respiratory Syndrome Coronavirus 2 (SARS-CoV-2). In December 2019, the first recorded case emerged in Wuhan, China [1]. Following the global spread of the virus, the World Health Organization (WHO) officially declared it a global pandemic on March 11, 2020.

Patients infected with SARS-CoV-2 may exhibit a range of symptoms and signs, from mild to severe. These can include fever, coughing, headaches, fatigue, sore throat, respiratory difficulties, anosmia (loss of smell), and ageusia (loss of taste) [1].

At this time, there is no precise, highly effective oral antiviral medication to treat COVID-19. Nonetheless, ongoing research is focused on fine-tuning various medications to advance a definitive cure for this global pandemic.

An effective approach in drug discovery involves assessing the efficacy of existing antiviral drugs for treating related viral diseases. Researchers conducted experiments with existing antiviral agents and obtained promising results in vitro for inhibiting the infection and transmission of 2019-nCoV. Among these antiviral compounds, you can find Remdesivir (GS5734), Chloroquine, Hydroxychloroquine, and Theaflavin [2-5]. Remdesivir is a

nucleotide analog drug with broad-spectrum activity that was originally developed to prevent Ebola virus infection [6, 7]. It has also demonstrated significant in vitro efficacy against 2019-nCoV [6]. Clinical trials are currently underway at multiple hospitals, and we eagerly anticipate results on their efficacy.

Chloroquine is a broad-spectrum antiviral drug widely used to treat malaria and autoimmune diseases [5, 8]. Numerous randomized controlled trials have been conducted to evaluate the impact of Chloroquine in the treatment of COVID-19, with reported therapeutic benefits including fever control, improved CT imaging, and delayed disease progression.

Hydroxychloroquine possesses antiviral activity that is closely similar to that of Chloroquine. Both drugs also exhibit immunomodulatory properties, which can enhance their antiviral efficacy in living organisms [9]. According to a Forbes report dated March 30, 2020, the FDA approved the use of Chloroquine and Hydroxychloroquine for emergency treatment of coronavirus. Hydroxychloroquine reduces the rapid progression of COVID-19 by suppressing the cytokine storm by inhibiting T-cell activation.

Theaflavin, a polyphenolic compound in black tea, is responsible for the health benefits of black tea consumption [10, 11]. Theaflavin has demonstrated broad-spectrum antiviral activity, effectively inhibiting viruses such as influenza A, influenza B, and hepatitis C. The study conducted by Lung et al. [2] discovered that Theaflavin holds promise as a primary candidate for developing an inhibitor against 2019-nCoV.

Using computer-based methodologies for the formation, amalgamation, and biological screening of compounds offers a more efficient alternative to the previous hit-and-miss approach in the intricate, expensive, and time-consuming process of drug discovery. In particular, QSPR/QSAR (quantitative structure-property relationship/quantitative structure-activity relationship) modeling plays a crucial role in understanding the physicochemical properties of molecules. Prior to a drug's introduction to the market, a substantial number of research trials are typically necessary to assess its tolerability, safety, and efficacy in the human body. These trials necessitate costly laboratory work, state-of-the-art facilities, and extensive experimentation. Researchers have established significant correlations between experiments on these compounds and their molecular graphs, providing insight into the physicochemical characteristics, bioactivities, and pharmacological behaviors of various chemical compounds. For more information, we refer to some recent articles [12-17].

Chemical graph theory (CGT) represents a significant field within mathematical chemistry that bridges the gap between the mathematical modeling of chemical compounds and the principles of graph theory. Within CGT, topological indices serve as numerical descriptors, providing insights into the molecular characteristics of compounds. These indices are widely used to predict physicochemical properties and biological activities through quantitative structure-property relationship (QSPR) and quantitative structure-activity relationship (QSAR) models [18-21].

Topological indices are classified according to structural attributes derived from the molecular graph. These classifications encompass distance-based indices [20, 22], which depend on distances between vertices; degree-based indices [23-30], which depend on vertex degrees; neighborhood degree sum-based indices [31, 32], which take into account the cumulative degrees of adjacent vertices; and spectral-value based indices [33, 34], which depends on the spectrum of the graph.

Traditionally, the computation of topological indices relied solely on their definitions, a process notorious for its time-consuming nature. Researchers have developed numerous

techniques to expedite the calculation of these indices. Notably, the polynomial representation of these indices has garnered significant attention in the literature. One prominent example is the Hosoya polynomial, also known as the Wiener polynomial [35, 36], which is used to compute various indices, including the Wiener index [37], the Hosoya index [38], and the Hyper Wiener index [39]. Another notable polynomial, the M-polynomial [40], serves as a versatile tool for determining at least nine degree-based topological indices [14, 41, 42].

Recently, Abhay and Lavanya introduced a series of topological indices, known as the “AL indices,” in the article [29]. They demonstrated that these AL indices have the highest discriminative power among both the set of octane isomers and the set of PCB molecules, compared with other vertex-degree-based indices. Furthermore, their research revealed that the AL indices exhibit a strong correlation with the physicochemical properties of octane and PCB molecules. To streamline the computation of these AL indices, we introduced the “ALM-Polynomial.” This polynomial serves a function analogous to the “M-Polynomial” [40] for degree-based indices. Additionally, we computed the “ALM-polynomial” for compounds, including Remdesivir, Chloroquine, Hydroxychloroquine, and Theaflavin.

A molecular graph of a chemical compound is created by transforming its atoms and chemical bonds into vertices and edges, respectively. Let’s define the ordered pair G as $(V(G), E(G))$, which represents a simple, connected, and undirected graph. In this context, $V(G)$ stands for the set of vertices, and $E(G)$ denotes the set of edges. Now, we define AL indices [29] for a molecular graph G .

For a given graph G , let $P_2(u)$ denote the number of distinct vertices at a distance two from vertex u .

$$AL_1(G) = \sum_{u \in V(G)} P_2(u) \tag{1}$$

$$AL_2(G) = \sum_{uv \in E(G)} \{P_2(u) + P_2(v)\} \tag{2}$$

$$AL_3(G) = \sum_{uv \in E(G)} P_2(u)P_2(v) \tag{3}$$

$$AL_4(G) = \sum_{uv \in E(G)} \sqrt{P_2(u)P_2(v)} \tag{4}$$

$$AL_5(G) = \sum_{uv \in E(G)} \frac{1}{\sqrt{P_2(u)P_2(v)}} \tag{5}$$

$$AL_6(G) = \sum_{uv \in E(G)} \left\{ \frac{P_2(u)}{P_2(v)} + \frac{P_2(v)}{P_2(u)} \right\} \tag{6}$$

$$AL_7(G) = \sum_{uv \in E(G)} \frac{P_2(u)P_2(v)}{P_2(u) + P_2(v)} \tag{7}$$

$$AL_8(G) = \sum_{uv \in E(G)} \frac{2}{P_2(u) + P_2(v)} \tag{8}$$

The relations of some AL topological indices with the ALM-polynomial are shown in Table 1.

2. Materials and Methods

Our primary objective is to provide a definition of ALM-polynomials, establish a connection with AL indices via certain calculus operators, and incorporate algebraic ALM-polynomials into the computation of topological indices for various antiviral drug structures. The second objective of this study is to assess novel AL indices for the antiviral compounds Remdesivir, Chloroquine, Hydroxychloroquine, and Theaflavin. To accomplish this, we first calculate the ALM-polynomials and subsequently derive the topological indices from these ALM-polynomials using calculus operators. In the concluding section of this article, we illustrate the geometric properties of ALM-polynomials and present numerical results, which are graphically compared in MATLAB 2015.

The chemical structures of Remdesivir, Chloroquine, Hydroxychloroquine, and Theaflavin were obtained from the following sources: <https://pubchem.ncbi.nlm.nih.gov/compound/5426> and the articles [13-16]. We focus on hydrogen-suppressed molecular graphs of the compounds, as hydrogen atoms' vertices do not contribute to graph isomorphism.

3. Results and Discussion

In this section, we give our main computational results and divide the section into two subsections.

3.1. The ALM-polynomial and its relationship with novel AL indices.

In this subsection, we provide the definition of the AL-polynomial and establish its relationship with novel AL indices using some calculus operators.

Definition 3.1 Let G be a molecular graph; then, the ALM-polynomial of graph G is defined as:

$$ALM(G, x, y) = \sum_{i \leq j} P_{ij} x^i y^j, \tag{9}$$

Where P_{ij} denotes the total number of edges $e = uv$ of G such that $P_2(u) = i$ and $P_2(v) = j$, where $P_2(u)$ denotes the number of distinct vertices at a distance of two from a fixed vertex u .

Now, we define the relationship between the $AL_2, AL_3, AL_4^\alpha, AL_5^\alpha, AL_6, AL_7,$ and AL_8 indices using certain calculus operators, as detailed in the article by Deutsch et al. [40]. This relationship is presented in Table 1.

Table 1. Short Description of AL indices, which depend on path length.

AL Index	The formula of topological indices	Derivation from $ALM(G, x, y)$
$AL_2(G)$	$\sum_{uv \in E(G)} \{P_2(u) + P_2(v)\}$	$(D_x + D_y)(ALM(G, x, y)) _{x=y=1}$
$AL_3(G)$	$\sum_{uv \in E(G)} P_2(u)P_2(v)$	$(D_x D_y)(ALM(G, x, y)) _{x=y=1}$
$AL_4^\alpha(G), \alpha \in \mathbb{N}$	$\sum_{uv \in E(G)} (P_2(u)P_2(v))^\alpha$	$(D_x^\alpha D_y^\alpha)(ALM(G, x, y)) _{x=y=1}$

AL Index	The formula of topological indices	Derivation from $ALM(G, x, y)$
$AL_5^\alpha(G)$, $\alpha \in \mathbb{N}$	$\sum_{uv \in E(G)} \frac{1}{(P_2(u)P_2(v))^\alpha}$	$(S_x^\alpha S_y^\alpha)(ALM(G, x, y)) _{x=y=1}$
$AL_6(G)$	$\sum_{uv \in E(G)} \left\{ \frac{P_2(u)}{P_2(v)} + \frac{P_2(v)}{P_2(u)} \right\}$	$(D_x S_y + D_y S_x)(ALM(G, x, y)) _{x=y=1}$
$AL_7(G)$	$\sum_{uv \in E(G)} \frac{P_2(u)P_2(v)}{P_2(u) + P_2(v)}$	$(S_x J D_x D_y)(ALM(G, x, y)) _{x=y=1}$
$AL_8(G)$	$\sum_{uv \in E(G)} \frac{2}{P_2(u) + P_2(v)}$	$(2S_x J)(ALM(G, x, y)) _{x=y=1}$

Where, $D_x f(x, y) = x \frac{\partial}{\partial x} f(x, y)$, $D_y f(x, y) = y \frac{\partial}{\partial y} f(x, y)$, $S_x f(x, y) = \int_0^x \frac{f(t, y)}{t} dt$, $S_y f(x, y) = \int_0^y \frac{f(x, t)}{t} dt$, $J(f(x, y)) = f(x, x)$.

We are now prepared to calculate topological indices for antiviral drugs using the ALM-polynomial.

3.2. Calculation of novel AL indices for antiviral drugs in the treatment of COVID-19 patients.

This section covers the calculation of various topological indices for antiviral drugs employed in the treatment of COVID-19 patients. The formulas expressing the relationships between $AL_2, AL_3, AL_4^\alpha, AL_5^\alpha, AL_6, AL_7$, and AL_8 indices and the ALM-polynomial are presented in Table 1.

Theorem 3.1 If G is a molecular graph of Remdesivir (GS – 5734), then:

$$ALM(G, x, y) = 2xy^2 + xy^3 + 2x^2y^2 + 9x^2y^3 + x^2y^4 + x^2y^5 + 9x^3y^3 + 3x^3y^4 + 7x^3y^5 + 2x^3y^6 + x^4y^4 + 2x^4y^5 + x^5y^5 + 3x^5y^6 + x^6y^6. \quad (10)$$

Proof 1. Let G represent the molecular graph of Remdesivir (depicted in Figure 1). This graph consists of 42 vertices and 45 edges. We define P_{ij} to be the count of edges $e = uv$ such that $P_2(u) = i$ and $P_2(v) = j$, denoted as $P_{ij} = \{uv \in E(G) : P_2(u) = i \text{ and } P_2(v) = j\}$.

From Figure 1, it is clear that. $P_{12} = 2, P_{13} = 1, P_{22} = 2, P_{23} = 9, P_{24} = 1, P_{25} = 1, P_{33} = 9, P_{34} = 3, P_{35} = 7, P_{36} = 2, P_{44} = 1, P_{45} = 2, P_{55} = 1, P_{56} = 3$, and $P_{66} = 1$. Now, utilizing these P_{ij} values in the definition of ALM-polynomial, we obtain:

$$ALM(G, x, y) = \sum_{i \leq j} P_{ij} x^i y^j = P_{12}xy^2 + P_{13}xy^3 + P_{22}x^2y^2 + P_{23}x^2y^3 + P_{24}x^2y^4 + P_{25}x^2y^5 + P_{33}x^3y^3 + P_{34}x^3y^4 + P_{35}x^3y^5 + P_{36}x^3y^6 + P_{44}x^4y^4 + P_{45}x^4y^5 + P_{55}x^5y^5 + P_{56}x^5y^6 + P_{66}x^6y^6. \quad (11)$$

By substituting the values of P_{ij} into Equation (11), we obtain:

$$ALM(G, x, y) = 2xy^2 + xy^3 + 2x^2y^2 + 9x^2y^3 + x^2y^4 + x^2y^5 + 9x^3y^3 + 3x^3y^4 + 7x^3y^5 + 2x^3y^6 + x^4y^4 + 2x^4y^5 + x^5y^5 + 3x^5y^6 + x^6y^6.$$



Figure 1. (a) represents the chemical structure of Remdesivir; (b) depicts the molecular graph of Remdesivir.

Using the ALM-polynomial, we calculate the novel AL indices based on path length two of Remdesivir (GS-5734) in the following theorem.

Theorem 3.2 Let G be the molecular graph of Remdesivir (GS – 5734). Then, we have:

1. $AL_2(G) = 306.$
2. $AL_3(G) = 552.$
3. $AL_4^\alpha(G) = 2(2)^\alpha + (3)^\alpha + 2(4)^\alpha + 9(6)^\alpha + (8)^\alpha + 9(9)^\alpha + (10)^\alpha + 3(12)^\alpha + 7(15)^\alpha + (16)^\alpha + 2(18)^\alpha + 2(20)^\alpha + (25)^\alpha + 3(30)^\alpha + (36)^\alpha.$
4. $AL_5^\alpha(G) = \frac{2}{(2)^\alpha} + \frac{1}{(3)^\alpha} + \frac{2}{(4)^\alpha} + \frac{9}{(6)^\alpha} + \frac{1}{(8)^\alpha} + \frac{9}{(9)^\alpha} + \frac{1}{(10)^\alpha} + \frac{3}{(12)^\alpha} + \frac{7}{(15)^\alpha} + \frac{2}{(18)^\alpha} + \frac{1}{(16)^\alpha} + \frac{2}{(20)^\alpha} + \frac{1}{(25)^\alpha} + \frac{3}{(30)^\alpha} + \frac{1}{(36)^\alpha}.$
5. $AL_6(G) = 98.550.$
6. $AL_7(G) = 73.5393.$
7. $AL_8(G) = 14.7105.$

Proof 2. Let $ALM(G, x, y) = \psi(x, y)$, then:

$$\psi(x, y) = 2xy^2 + xy^3 + 2x^2y^2 + 9x^2y^3 + x^2y^4 + x^2y^5 + 9x^3y^3 + 3x^3y^4 + 7x^3y^5 + 2x^3y^6 + x^4y^4 + 2x^4y^5 + x^5y^5 + 3x^5y^6 + x^6y^6.$$

Now, to calculate the AL indices based on path length two, we need the following terms:

$$D_x\psi(x, y) = x \frac{\partial}{\partial x} \psi(x, y) = 2xy^2 + xy^3 + 4x^2y^2 + 18x^2y^3 + 2x^2y^4 + 2x^2y^5 + 27x^3y^3 + 9x^3y^4 + 21x^3y^5 + 6x^3y^6 + 4x^4y^4 + 8x^4y^5 + 5x^5y^5 + 15x^5y^6 + 6x^6y^6. \quad (12)$$

$$D_y\psi(x, y) = y \frac{\partial}{\partial y} \psi(x, y) = 4xy^2 + 3xy^3 + 4x^2y^2 + 27x^2y^3 + 4x^2y^4 + 5x^2y^5 + 27x^3y^3 + 12x^3y^4 + 35x^3y^5 + 12x^3y^6 + 4x^4y^4 + 10x^4y^5 + 5x^5y^5 + 18x^5y^6 + 6x^6y^6. \quad (13)$$

$$D_xD_y\psi(x, y) = 4xy^2 + 3xy^3 + 8x^2y^2 + 54x^2y^3 + 8x^2y^4 + 10x^2y^5 + 81x^3y^3 + 36x^3y^4 + 105x^3y^5 + 36x^3y^6 + 16x^4y^4 + 40x^4y^5 + 25x^5y^5 + 90x^5y^6 + 36x^6y^6. \quad (14)$$

$$D_x^\alpha\psi(x, y) = 2(2)^\alpha xy^2 + (3)^\alpha xy^3 + 2(2)^\alpha x^2y^2 + 9(3)^\alpha x^2y^3 + (4)^\alpha x^2y^4 + (5)^\alpha x^2y^5 + 9(3)^\alpha x^3y^3 + 3(4)^\alpha x^3y^4 + 7(5)^\alpha x^3y^5 + 2(6)^\alpha x^3y^6 + (4)^\alpha x^4y^4 + 2(5)^\alpha x^4y^5 + (5)^\alpha x^5y^5 + 3(6)^\alpha x^5y^6 + (6)^\alpha x^6y^6. \quad (15)$$

$$D_x^\alpha D_y^\alpha\psi(x, y) = 2(2)^\alpha xy^2 + (3)^\alpha xy^3 + 2(4)^\alpha x^2y^2 + 9(6)^\alpha x^2y^3 + (8)^\alpha x^2y^4 + (10)^\alpha x^2y^5 + 9(9)^\alpha x^3y^3 + 3(12)^\alpha x^3y^4 + 7(15)^\alpha x^3y^5 + 2(18)^\alpha x^3y^6 + (16)^\alpha x^4y^4 + 2(20)^\alpha x^4y^5 + (25)^\alpha x^5y^5 + 3(30)^\alpha x^5y^6 + (36)^\alpha x^6y^6. \quad (16)$$

$$\begin{aligned}
 S_x \psi(x, y) &= \int_0^x \frac{\psi(t, y)}{t} dt \\
 &= 2xy^2 + xy^3 + x^2y^2 + \frac{9}{2}x^2y^3 + \frac{1}{2}x^2y^4 + \frac{1}{2}x^2y^5 + 3x^3y^3 + x^3y^4 \\
 &\quad + \frac{7}{3}x^3y^5 + \frac{2}{3}x^3y^6 + \frac{1}{4}x^4y^4 + \frac{1}{2}x^4y^5 + \frac{1}{5}x^5y^5 + \frac{3}{5}x^5y^6 + \frac{1}{6}x^6y^6. \quad (17)
 \end{aligned}$$

$$\begin{aligned}
 S_y \psi(x, y) &= \int_0^y \frac{\psi(x, t)}{t} dt \\
 &= xy^2 + \frac{1}{3}xy^3 + x^2y^2 + 3x^2y^3 + \frac{1}{4}x^2y^4 + \frac{1}{5}x^2y^5 + 3x^3y^3 + \frac{3}{4}x^3y^4 \\
 &\quad + \frac{7}{5}x^3y^5 + \frac{1}{3}x^3y^6 + \frac{1}{4}x^4y^4 + \frac{2}{5}x^4y^5 + \frac{1}{5}x^5y^5 + \frac{1}{2}x^5y^6 + \frac{1}{6}x^6y^6. \quad (18)
 \end{aligned}$$

$$\begin{aligned}
 S_y^\alpha \psi(x, y) &= \frac{2}{2^\alpha}xy^2 + \frac{1}{3^\alpha}xy^3 + \frac{2}{2^\alpha}x^2y^2 + \frac{9}{3^\alpha}x^2y^3 + \frac{1}{4^\alpha}x^2y^4 + \frac{1}{5^\alpha}x^2y^5 + \frac{9}{3^\alpha}x^3y^3 \\
 &\quad + \frac{3}{4^\alpha}x^3y^4 + \frac{7}{5^\alpha}x^3y^5 + \frac{2}{6^\alpha}x^3y^6 + \frac{1}{4^\alpha}x^4y^4 + \frac{2}{5^\alpha}x^4y^5 + \frac{1}{5^\alpha}x^5y^5 + \frac{3}{6^\alpha}x^5y^6 \\
 &\quad + \frac{1}{6^\alpha}x^6y^6. \quad (19)
 \end{aligned}$$

$$\begin{aligned}
 S_x^\alpha S_y^\alpha \psi(x, y) &= \frac{2}{2^\alpha}xy^2 + \frac{1}{3^\alpha}xy^3 + \frac{2}{4^\alpha}x^2y^2 + \frac{9}{6^\alpha}x^2y^3 + \frac{1}{8^\alpha}x^2y^4 + \frac{1}{10^\alpha}x^2y^5 + \frac{9}{9^\alpha}x^3y^3 \\
 &\quad + \frac{3}{12^\alpha}x^3y^4 + \frac{7}{15^\alpha}x^3y^5 + \frac{2}{18^\alpha}x^3y^6 + \frac{1}{16^\alpha}x^4y^4 + \frac{2}{20^\alpha}x^4y^5 + \frac{1}{25^\alpha}x^5y^5 \\
 &\quad + \frac{3}{30^\alpha}x^5y^6 + \frac{1}{36^\alpha}x^6y^6. \quad (20)
 \end{aligned}$$

$$\begin{aligned}
 D_x S_y \psi(x, y) &= xy^2 + \frac{1}{3}xy^3 + 2x^2y^2 + 6x^2y^3 + \frac{1}{2}x^2y^4 + \frac{2}{5}x^2y^5 + 9x^3y^3 + \frac{9}{4}x^3y^4 \\
 &\quad + \frac{21}{5}x^3y^5 + x^3y^6 + x^4y^4 + \frac{8}{5}x^4y^5 + x^5y^5 + \frac{5}{2}x^5y^6 + x^6y^6. \quad (21)
 \end{aligned}$$

$$\begin{aligned}
 D_y S_x \psi(x, y) &= 4xy^2 + 3xy^3 + 2x^2y^2 + \frac{27}{2}x^2y^3 + 2x^2y^4 + \frac{5}{2}x^2y^5 + 9x^3y^3 + 4x^3y^4 \\
 &\quad + \frac{35}{3}x^3y^5 + 4x^3y^6 + x^4y^4 + \frac{5}{2}x^4y^5 + x^5y^5 + \frac{18}{5}x^5y^6 + x^6y^6. \quad (22)
 \end{aligned}$$

$$J(\psi(x, y)) = 2x^3 + 3x^4 + 9x^5 + 10x^6 + 4x^7 + 8x^8 + 4x^9 + x^{10} + 3x^{11} + x^{12}. \quad (23)$$

$$\begin{aligned}
 S_x J(\psi(x, y)) &= \frac{2}{3}x^3 + \frac{3}{4}x^4 + \frac{9}{5}x^5 + \frac{5}{3}x^6 + \frac{4}{7}x^7 + x^8 + \frac{4}{9}x^9 + \frac{1}{10}x^{10} + \frac{3}{11}x^{11} \\
 &\quad + \frac{1}{12}x^{12}. \quad (24)
 \end{aligned}$$

$$\begin{aligned}
 JD_x D_y(\psi(x, y)) &= 4x^3 + 11x^4 + 54x^5 + 89x^6 + 46x^7 + 121x^8 + 76x^9 + 25x^{10} \\
 &\quad + 90x^{11} + 36x^{12}. \quad (25)
 \end{aligned}$$

$$S_x J D_x D_y (\psi(x, y)) = \frac{4}{3}x^3 + \frac{11}{4}x^4 + \frac{54}{5}x^5 + \frac{89}{6}x^6 + \frac{46}{7}x^7 + \frac{121}{8}x^8 + \frac{76}{9}x^9 + \frac{25}{10}x^{10} + \frac{90}{11}x^{11} + 3x^{12}. \quad (26)$$

Now, by employing the derivative formulas provided in Equations 12–26 for the AL topological indices listed in Table 1, we obtain the required results:

$$AL_2(G) = (D_x + D_y)(\psi(x, y))|_{x=y=1} = 306,$$

$$AL_3(G) = (D_x \cdot D_y)(\psi(x, y))|_{x=y=1} = 552,$$

$$AL_4^\alpha(G) = (D_x^\alpha D_y^\alpha)(\psi(x, y))|_{x=y=1} = 2(2)^\alpha + (3)^\alpha + 2(4)^\alpha + 9(6)^\alpha + (8)^\alpha + 9(9)^\alpha + (10)^\alpha + 3(12)^\alpha + 7(15)^\alpha + (16)^\alpha + 2(18)^\alpha + 2(20)^\alpha + (25)^\alpha + 3(30)^\alpha + (36)^\alpha,$$

$$AL_5^\alpha(G) = (S_x^\alpha S_y^\alpha)(\psi(x, y))|_{x=y=1} = \frac{2}{(2)^\alpha} + \frac{1}{(3)^\alpha} + \frac{2}{(4)^\alpha} + \frac{9}{(6)^\alpha} + \frac{1}{(8)^\alpha} + \frac{9}{(9)^\alpha} + \frac{1}{(10)^\alpha} + \frac{3}{(12)^\alpha} + \frac{7}{(15)^\alpha} + \frac{2}{(18)^\alpha} + \frac{1}{(16)^\alpha} + \frac{2}{(20)^\alpha} + \frac{1}{(25)^\alpha} + \frac{3}{(30)^\alpha} + \frac{1}{(36)^\alpha},$$

$$AL_6(G) = (D_x S_y + D_y S_x)(\psi(x, y))|_{x=y=1} = 98.550,$$

$$AL_7(G) = (S_x J D_x D_y)(\psi(x, y))|_{x=y=1} = 73.5393,$$

$$AL_8(G) = (2S_x J)(\psi(x, y))|_{x=y=1} = 14.7105.$$

We evaluate the ALM-polynomial of the molecular graph of Chloroquine in the following theorem.

Theorem 3.3 Let G be the molecular graph of Chloroquine (Figure 2), then we have:

$$ALM(G, x, y) = 2xy^2 + 2x^2y^2 + 8x^2y^3 + 2x^2y^4 + 2x^3y^3 + 2x^3y^4 + x^3y^5 + 2x^4y^4 + 2x^4y^5. \quad (27)$$

Proof 3. Consider the molecular graph G of Chloroquine, which consists of 22 vertices and 23 edges, as illustrated in Figure 2. From the figure, we can deduce the following values: $P_{12} = 2, P_{22} = 2, P_{23} = 8, P_{24} = 2, P_{33} = 2, P_{34} = 2, P_{35} = 1, P_{44} = 2,$ and $P_{45} = 2$. Now, by substituting these P_{ij} values into the definition of ALM-polynomial, we have:

$$ALM(G, x, y) = 2xy^2 + 2x^2y^2 + 8x^2y^3 + 2x^2y^4 + 2x^3y^3 + 2x^3y^4 + x^3y^5 + 2x^4y^4 + 2x^4y^5.$$

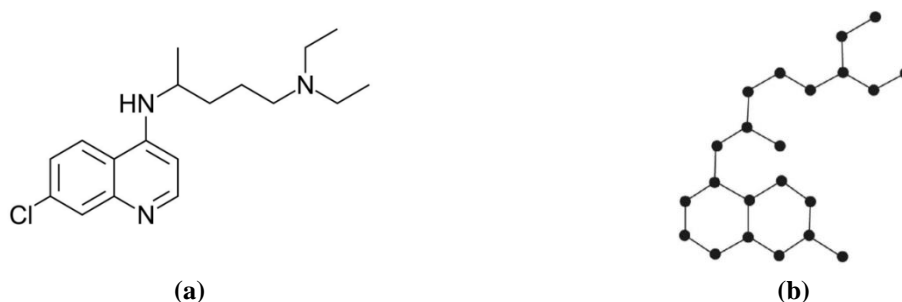


Figure 2. (a) represents the chemical structure of Chloroquine; (b) depicts the molecular graph of Chloroquine.

Now, utilizing the ALM-polynomial, we calculate the AL indices for Chloroquine, as presented in the following theorem.

Theorem 3.4 Let G represent the molecular graph of Chloroquine. Then, we have:

1. $AL_2(G) = 134.$
2. $AL_3(G) = 205.$

3. $AL_4^\alpha(G) = 2(2)^\alpha + 2(4)^\alpha + 8(6)^\alpha + 2(8)^\alpha + 2(9)^\alpha + 2(12)^\alpha + (15)^\alpha + 2(16)^\alpha + 2(20)^\alpha.$
4. $AL_5^\alpha(G) = \frac{2}{(2)^\alpha} + \frac{2}{(4)^\alpha} + \frac{8}{(6)^\alpha} + \frac{2}{(8)^\alpha} + \frac{2}{(9)^\alpha} + \frac{2}{(12)^\alpha} + \frac{1}{(15)^\alpha} + \frac{2}{(16)^\alpha} + \frac{2}{(20)^\alpha}.$
5. $AL_6(G) = 49.866.$
6. $AL_7(G) = 32.348.$
7. $AL_8(G) = 8.632.$

Proof 4. The proof follows a similar pattern to Theorem 3.2.

ALM-polynomial of the molecular graph of Hydroxychloroquine is evaluated in the following theorem.

Theorem 3.5 Let G represent the molecular graph of Hydroxychloroquine (depicted in Figure 3). Then, we have:

$$ALM(G, x, y) = xy + xy^2 + xy^3 + 2x^2y^2 + 7x^2y^3 + 2x^2y^4 + 3x^3y^3 + 2x^3y^4 + x^3y^5 + 2x^4y^4 + 2x^4y^5. \quad (28)$$

Proof 5. Let G be the molecular graph of Hydroxychloroquine. It has 23 vertices and 24 edges. Observing Figure 3, we can deduce the following values: $P_{11} = 1, P_{12} = 1, P_{13} = 1, P_{22} = 2, P_{23} = 7, P_{24} = 2, P_{33} = 3, P_{34} = 2, P_{35} = 1, P_{44} = 2,$ and $P_{45} = 2.$ Now, we are utilizing these P_{ij} values in the definition of ALM-polynomial, we obtain:

$$ALM(G, x, y) = xy + xy^2 + xy^3 + 2x^2y^2 + 7x^2y^3 + 2x^2y^4 + 3x^3y^3 + 2x^3y^4 + x^3y^5 + 2x^4y^4 + 2x^4y^5.$$

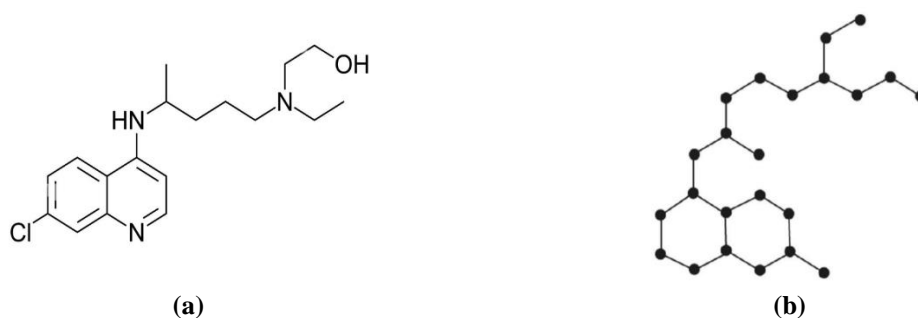


Figure 3. (a) represents the chemical structure of Hydroxychloroquine; (b) depicts the molecular graph of Hydroxychloroquine.

Using the ALM-polynomial, we compute the AL indices for Hydroxychloroquine, as detailed in the following theorem.

Theorem 3.6 Let G represent the molecular graph of Hydroxychloroquine. Then, we have:

1. $AL_2(G) = 138.$
2. $AL_3(G) = 210.$
3. $AL_4^\alpha(G) = 1 + (2)^\alpha + (3)^\alpha + 2(4)^\alpha + 7(6)^\alpha + 2(8)^\alpha + 3(9)^\alpha + 2(12)^\alpha + (15)^\alpha + 2(16)^\alpha + 2(20)^\alpha.$
4. $AL_5^\alpha(G) = 1 + \frac{1}{(2)^\alpha} + \frac{1}{(3)^\alpha} + \frac{2}{(4)^\alpha} + \frac{7}{(6)^\alpha} + \frac{2}{(8)^\alpha} + \frac{3}{(9)^\alpha} + \frac{2}{(12)^\alpha} + \frac{1}{(15)^\alpha} + \frac{2}{(16)^\alpha} + \frac{2}{(20)^\alpha}.$
5. $AL_6(G) = 52.533.$
6. $AL_7(G) = 33.231.$
7. $AL_8(G) = 9.399.$

Proof 6. The proof follows a similar pattern to Theorem 3.2.

In the following theorem, we calculate the ALM-polynomial for the molecular graph of Theaflavin.

Theorem 3.7 Let G represent the molecular graph of Theaflavin. Then, we have:

$$ALM(G, x, y) = 2x^2y^2 + 6x^2y^3 + 6x^2y^4 + 8x^3y^4 + 4x^3y^5 + 6x^4y^4 + 9x^4y^5 + 2x^4y^6 + 2x^5y^5 + x^5y^6. \quad (29)$$

Proof 7. Let G represent the molecular graph of Theaflavin (depicted in Figure 4). This graph contains 41 vertices and 46 edges. Observing Figure 4, we can deduce the following values: $P_{22} = 2, P_{23} = 6, P_{24} = 6, P_{34} = 8, P_{35} = 4, P_{44} = 6, P_{45} = 9, P_{46} = 2, P_{55} = 2,$ and $P_{56} = 1$. Now, we are utilizing these P_{ij} values in the definition of ALM-polynomial, we obtain

$$ALM(G, x, y) = 2x^2y^2 + 6x^2y^3 + 6x^2y^4 + 8x^3y^4 + 4x^3y^5 + 6x^4y^4 + 9x^4y^5 + 2x^4y^6 + 2x^5y^5 + x^5y^6.$$

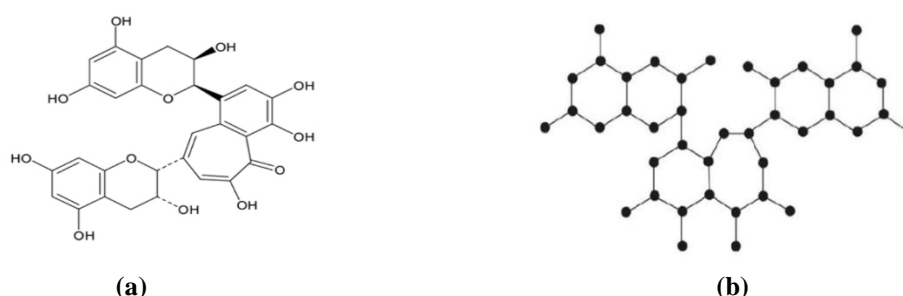


Figure 4. (a) represents the chemical structure of Theaflavin; (b) depicts the molecular graph of Theaflavin.

Now, using the ALM-polynomial, we compute the AL indices for Theaflavin in the following theorem.

Theorem 3.8 Let G represent the molecular graph of Theaflavin. Then, we have:

1. $AL_2(G) = 342$.
2. $AL_3(G) = 652$.
3. $AL_4^\alpha(G) = 2(4)^\alpha + 6(6)^\alpha + 6(8)^\alpha + 8(12)^\alpha + 4(15)^\alpha + 6(16)^\alpha + 9(20)^\alpha + 2(24)^\alpha + 2(25)^\alpha + (30)^\alpha$.
4. $AL_5^\alpha(G) = \frac{2}{(4)^\alpha} + \frac{6}{(6)^\alpha} + \frac{6}{(8)^\alpha} + \frac{8}{(12)^\alpha} + \frac{4}{(15)^\alpha} + \frac{6}{(16)^\alpha} + \frac{9}{(20)^\alpha} + \frac{2}{(24)^\alpha} + \frac{2}{(25)^\alpha} + \frac{1}{(30)^\alpha}$.
5. $AL_6(G) = 98.550$.
6. $AL_7(G) = 82.941$.
7. $AL_8(G) = 13.167$.

Proof 8. The proof follows a similar pattern to Theorem 3.2.

4. Graphical Illustrations of ALM-polynomial, AL_4^α , and AL_5^α Indices

Figures 5(a)–5(d) present the three-dimensional (3-D) plots of the ALM-polynomials for Remdesivir, Chloroquine, Hydroxychloroquine, and Theaflavin, respectively. All four surfaces exhibit smooth and strictly increasing behavior over the positive x – y domain, as each ALM-polynomial consists of positive coefficients and non-negative powers of x and y . The ALM surface for Remdesivir in Figure 5(a) shows a steep rise, particularly for larger values of x and y , due to the presence of multiple higher-degree mixed terms. In contrast, Figure 5(b), corresponding to Chloroquine, displays a comparatively gentler surface, reflecting fewer higher-order terms and smaller coefficients. The surface for Hydroxychloroquine in Figure 5(c) demonstrates intermediate growth, lying between those of Chloroquine and Remdesivir across the same domain. Meanwhile, Figure 5(d) for Theaflavin exhibits a rapidly increasing surface with a pronounced elevation in the higher x – y region, driven by dominant higher-degree terms with larger multiplicities. Overall, the comparative analysis of Figures 5(a)–5(d) indicates that

Theaflavin and Remdesivir attain higher ALM values, while Hydroxychloroquine and Chloroquine show relatively lower magnitudes, highlighting clear structural distinctions among the studied drug molecules.

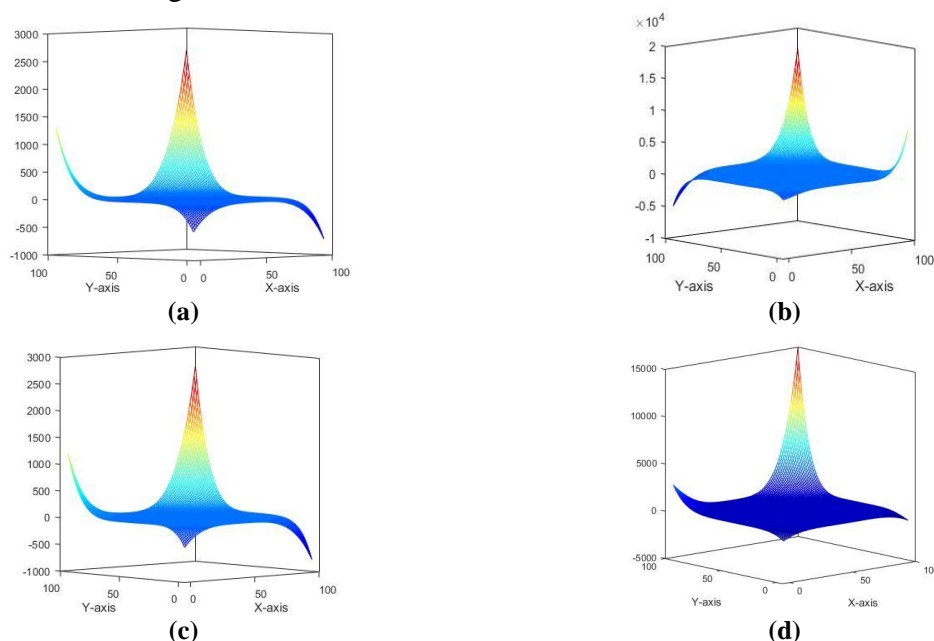
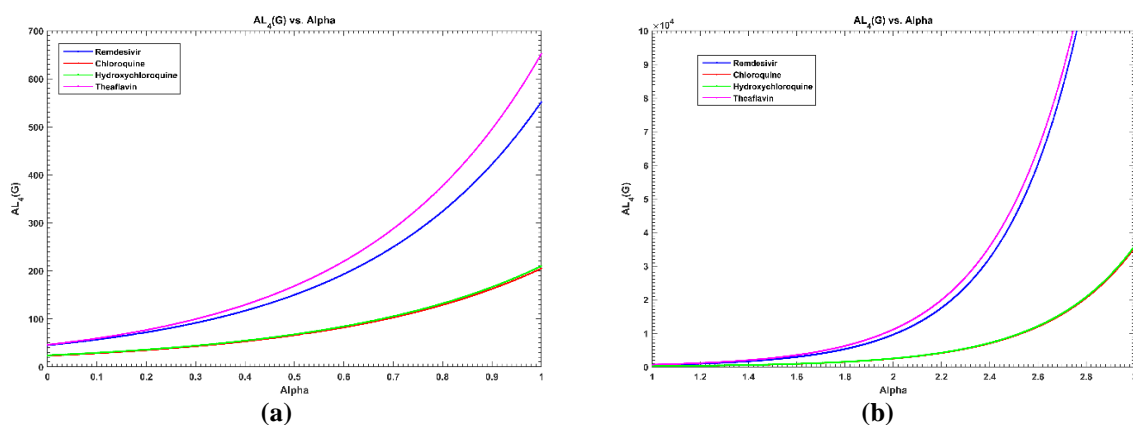


Figure 5. 3-D plot of the ALM-polynomial for Remdesivir, Chloroquine, Hydroxychloroquine, and Theaflavin.

Figure 6 collectively illustrates the variation of the indices AL_4^α and AL_5^α for Remdesivir, Chloroquine, Hydroxychloroquine, and Theaflavin with respect to the parameter α . Figures 6(a) and 6(b) depict the behavior of AL_4^α in the intervals $0 \leq \alpha \leq 1$ and $\alpha > 1$, respectively, while Figures 6(c) and 6(d) present the corresponding variation of AL_5^α over the same parameter ranges. In both regions, the AL_4^α curves exhibit a monotonic increase with increasing α , reflecting the presence of positive coefficients and positive base terms raised to the power α . Conversely, the AL_5^α curves display a monotonic decreasing trend, as they are composed of reciprocal power terms of the form $1/k^\alpha$. For smaller values of α , the variations in both indices are relatively gradual, whereas for larger values of α , the influence of higher-degree terms becomes more pronounced, leading to sharper divergence among the curves. Across all parameter ranges, Theaflavin consistently shows the highest values, followed by Remdesivir, while Hydroxychloroquine and Chloroquine exhibit comparatively lower values. This combined graphical analysis demonstrates the complementary behavior of AL_4^α and AL_5^α and highlights their effectiveness in differentiating the structural properties of the studied drug molecules.



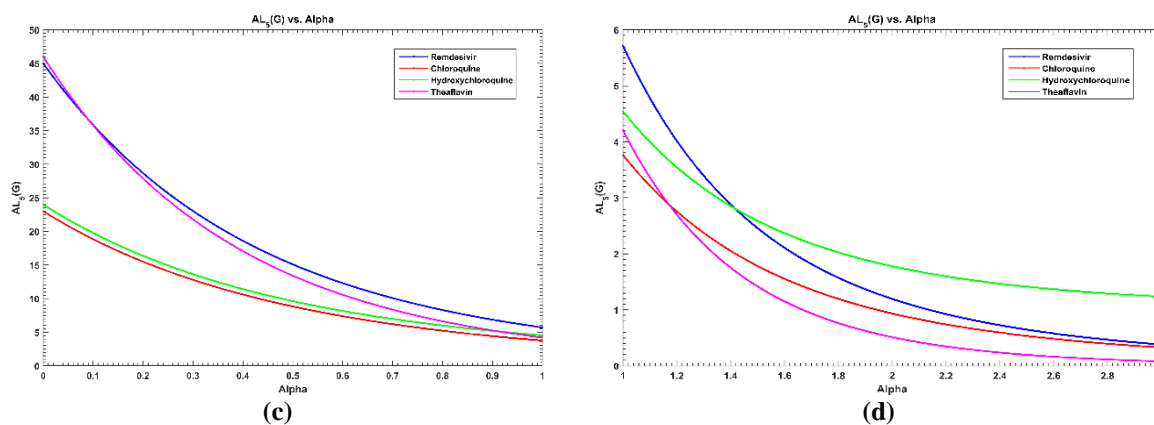


Figure 6. AL_4^α , AL_5^α for different ranges of alpha value.

5. Conclusion

In this article, we conducted a study of the topological properties of chemical structures used to inhibit the outbreak and transmission of COVID-19. These structures include Remdesivir (GS-5734), Chloroquine, Hydroxychloroquine, and Theaflavin. Our focus has been on the novel AL indices, which depend on path length. By introducing the ALM-polynomial and applying it to these compounds, we were able to calculate and evaluate various topological indices, such as “ $AL_2(G)$, $AL_3(G)$, $AL_4^\alpha(G)$, $AL_5^\alpha(G)$, $AL_6(G)$, $AL_7(G)$ and $AL_8(G)$ ”. To facilitate a better understanding of our findings, we have also provided graphical representations of the results. These outcomes offer valuable insights into the structural characteristics of the aforementioned compounds. It’s worth noting that topological indices have the capacity to predict diverse properties and activities, such as boiling point, entropy, enthalpy, acentric factor, critical pressure, and more. As such, our discoveries hold promise for guiding the development of new drugs and vaccines for the treatment of COVID-19.

Author Contributions

Conceptualization, A.R.; methodology, A.R.; formal analysis, A.R.; investigation, A.R.; data curation, A.R.; writing—original draft preparation, A.R.; writing—review and editing, A.R.; visualization, A.R. All authors have read and agreed to the published version of the manuscript.

Institutional Review Board Statement

Not applicable.

Informed Consent Statement

Not applicable.

Data Availability Statement

Data supporting the findings of this study are available upon reasonable request from the corresponding author.

Funding

This research received no external funding.

Acknowledgments

The author sincerely thanks the reviewers and the editor for their valuable suggestions and constructive comments, which significantly improved the quality and clarity of this manuscript.

Conflicts of Interest

The authors declare no conflict of interest.

References

1. Huang, C.; Wang, Y.; Li, X.; Ren, L.; Zhao, J.; Hu, Y.; Zhang, L.; Fan, G.; Xu, J.; Gu, X.; Cheng, Z.; Yu, T.; Xia, J.; Wei, Y.; Wu, W.; Xie, X.; Yin, W.; Li, H.; Liu, M.; Xiao, Y.; Gao, H.; Guo, L.; Xie, J.; Wang, G.; Jiang, R.; Gao, Z.; Jin, Q.; Wang, J.; Cao, B. Clinical features of patients infected with 2019 novel coronavirus in Wuhan, China. *Lancet* **2020**, *395*, 497-506, [https://doi.org/10.1016/s0140-6736\(20\)30183-5](https://doi.org/10.1016/s0140-6736(20)30183-5).
2. Lung, J.; Lin, Y.-S.; Yang, Y.-H.; Chou, Y.-L.; Shu, L.-H.; Cheng, Y.-C.; Liu, H.T.; Wu, C.-Y. The potential chemical structure of anti-SARS-CoV-2 RNA-dependent RNA polymerase. *J. Med. Virol.* **2020**, *92*, 693-697, <https://doi.org/10.1002/jmv.25761>.
3. Morse, J.S.; Lalonde, T.; Xu, S.; Liu, W.R. Learning from the Past: Possible Urgent Prevention and Treatment Options for Severe Acute Respiratory Infections Caused by 2019-nCoV. *ChemBioChem* **2020**, *21*, 730-738, <https://doi.org/10.1002/cbic.202000047>.
4. Wang, M.; Cao, R.; Zhang, L.; Yang, X.; Liu, J.; Xu, M.; Shi, Z.; Hu, Z.; Zhong, W.; Xiao, G. Remdesivir and Chloroquine effectively inhibit the recently emerged novel coronavirus (2019-nCoV) in vitro. *Cell Res.* **2020**, *30*, 269-271, <https://doi.org/10.1038/s41422-020-0282-0>.
5. Zhou, D.; Dai, S.-M.; Tong, Q. COVID-19: a recommendation to examine the effect of Hydroxychloroquine in preventing infection and progression. *J. Antimicrob. Chemother.* **2020**, *75*, 1667-1670, <https://doi.org/10.1093/jac/dkaa114>.
6. Siegel, D.; Hui, H.C.; Doerffler, E.; Clarke, M.O.; Chun, K.; Zhang, L.; Neville, S.; Carra, E.; Lew, W.; Ross, B.; Wang, Q.; Wolfe, L.; Jordan, R.; Soloveva, V.; Knox, J.; Perry, J.; Perron, M.; Stray, K.M.; Barauskas, O.; Feng, J.Y.; Xu, Y.; Lee, G.; Rheingold, A.L.; Ray, A.S.; Bannister, R.; Strickley, R.; Swaminathan, S.; Lee, W.A.; Bavari, S.; Cihlar, T.; Lo, M.K.; Warren, T.K.; Mackman, R.L. Discovery and Synthesis of a Phosphoramidate Prodrug of a Pyrrolo[2,1-f][triazin-4-amino] Adenine C-Nucleoside (GS-5734) for the Treatment of Ebola and Emerging Viruses. *J. Med. Chem.* **2017**, *60*, 1648-1661, <https://doi.org/10.1021/acs.jmedchem.6b01594>.
7. Warren, T.K.; Jordan, R.; Lo, M.K.; Ray, A.S.; Mackman, R.L.; Soloveva, V.; Siegel, D.; Perron, M.; Bannister, R.; Hui, H.C.; Larson, N.; Strickley, R.; Wells, J.; Stuthman, K.S.; Van Tongeren, S.A.; Garza, N.L.; Donnelly, G.; Shurtleff, A.C.; Retterer, C.J.; Gharabeh, D.; Zamani, R.; Kenny, T.; Eaton, B.P.; Grimes, E.; Welch, L.S.; Gomba, L.; Wilhelmsen, C.L.; Nichols, D.K.; Nuss, J.E.; Nagle, E.R.; Kugelman, J.R.; Palacios, G.; Doerffler, E.; Neville, S.; Carra, E.; Clarke, M.O.; Zhang, L.; Lew, W.; Ross, B.; Wang, Q.; Chun, K.; Wolfe, L.; Babusis, D.; Park, Y.; Stray, K.M.; Trancheva, I.; Feng, J.Y.; Barauskas, O.; Xu, Y.; Wong, P.; Braun, M.R.; Flint, M.; McMullan, L.K.; Chen, S.-S.; Fearn, R.; Swaminathan, S.; Mayers, D.L.; Spiropoulou, C.F.; Lee, W.A.; Nichol, S.T.; Cihlar, T.; Bavari, S. Therapeutic efficacy of the small molecule GS-5734 against Ebola virus in rhesus monkeys. *Nature* **2016**, *531*, 381-385, <https://doi.org/10.1038/nature17180>.
8. Savarino, A.; Di Trani, L.; Donatelli, I.; Cauda, R.; Cassone, A. New insights into the antiviral effects of Chloroquine. *Lancet Infect. Dis.* **2006**, *6*, 67-69, [https://doi.org/10.1016/s1473-3099\(06\)70361-9](https://doi.org/10.1016/s1473-3099(06)70361-9).
9. Ejuh, G.W.; Fonkem, C.; Tadjouteu Assatse, Y.; Yossa Kamsi, R.A.; Nya, T.; Ndikum, L.P.; Ndjaka, J.M.B. Study of the structural, chemical descriptors and optoelectronic properties of the drugs Hydroxychloroquine and Azithromycin. *Heliyon* **2020**, *6*, e04647, <https://doi.org/10.1016/j.heliyon.2020.e04647>.
10. Chowdhury, P.; Sahuc, M.-E.; Rouillé, Y.; Rivière, C.; Bonneau, N.; Vandeputte, A.; Brodin, P.; Goswami, M.; Bandyopadhyay, T.; Dubuisson, J.; Séron, K. Theaflavins, polyphenols of black tea, inhibit entry of hepatitis C virus in cell culture. *PLOS ONE* **2018**, *13*, e0198226, <https://doi.org/10.1371/journal.pone.0198226>.

11. Yang, Z.-F.; Bai, L.-P.; Huang, W.-b.; Li, X.-Z.; Zhao, S.-S.; Zhong, N.-S.; Jiang, Z.-H. Comparison of in vitro antiviral activity of tea polyphenols against influenza A and B viruses and structure–activity relationship analysis. *Fitoterapia* **2014**, *93*, 47–53, <https://doi.org/10.1016/j.fitote.2013.12.011>.
12. Çolakoglu, Ö. QSPR Modeling with Topological Indices of Some Potential Drug Candidates against COVID-19. *J. Math.* **2022**, *2022*, 3785932, <https://doi.org/10.1155/2022/3785932>.
13. Das, S.; Rai, S.; Kumar, V. On topological indices of Molnupiravir and its QSPR modelling with some other antiviral drugs to treat COVID-19 patients. *J. Math. Chem.* **2023**, 1–44, <https://doi.org/10.1007/s10910-023-01518-z>.
14. Havare, Ö.Ç. Topological indices and QSPR modeling of some novel drugs used in the cancer treatment. *Int. J. Quantum Chem.* **2021**, *121*, e26813, <https://doi.org/10.1002/qua.26813>.
15. Mondal, S.; De, N.; Pal, A. Topological Indices of Some Chemical Structures Applied for the Treatment of COVID-19 Patients. *Polycyclic Aromat. Compd.* **2022**, *42*, 1220–1234, <https://doi.org/10.1080/10406638.2020.1770306>.
16. Rauf, A.; Naeem, M.; Hanif, A. Quantitative structure–properties relationship analysis of Eigen-value-based indices using COVID-19 drugs structure. *Int. J. Quantum Chem.* **2023**, *123*, e27030, <https://doi.org/10.1002/qua.27030>.
17. Rosary, M.S. Topological Study of Line Graph of Remdesivir Compound Used in the Treatment of Corona Virus. *Polycyclic Aromat. Compd.* **2022**, *42*, 5731–5747, <https://doi.org/10.1080/10406638.2021.1956552>.
18. Basak, S.C. Use of Graph Invariants in Quantitative Structure–Activity Relationship Studies. *Croat. Chem. Acta* **2016**, *89*, 419–429, <http://dx.doi.org/10.5562/cca3029>.
19. Gutman, I. Degree-Based Topological Indices. *Croat. Chem. Acta* **2013**, *86*, 351–361, <http://dx.doi.org/10.5562/cca2294>.
20. Gutman, I.; Trinajstić, N. Graph theory and molecular orbitals. Total ϕ -electron energy of alternant hydrocarbons. *Chem. Phys. Lett.* **1972**, *17*, 535–538, [https://doi.org/10.1016/0009-2614\(72\)85099-1](https://doi.org/10.1016/0009-2614(72)85099-1).
21. Rauf, A.; Ishtiaq, M.; Siddiqui, M.K. Topological Study of Hydroxychloroquine Conjugated Molecular Structure Used for Novel Coronavirus (COVID-19) Treatment. *Polycyclic Aromat. Compd.* **2022**, *42*, 3792–3808, <https://doi.org/10.1080/10406638.2021.1873807>.
22. Bozkurt Altındağ, Ş.B.; Milovanović, I.Ž.; Milovanović, E.I.; Matejić, M.M. Modified hyper-Wiener index of trees. *Discret. Appl. Math.* **2023**, *334*, 101–109, <https://doi.org/10.1016/j.dam.2023.03.005>.
23. Ali, A.; Elumalai, S.; Mansour, T. On the Symmetric Division Deg Index of Molecular Graphs. *MATCH Commun. Math. Comput. Chem.* **2020**, *83*, 205–220.
24. Ali, A.; Zhong, L.; Gutman, I. Harmonic Index and its Generalizations: Extremal Results and Bounds. *MATCH Commun. Math. Comput. Chem.* **2019**, *81*, 249–311.
25. Furtula, B.; Ch. Das, K.; Gutman, I. Comparative analysis of symmetric division deg index as potentially useful molecular descriptor. *Int. J. Quantum Chem.* **2018**, *118*, e25659, <https://doi.org/10.1002/qua.25659>.
26. Liu, H. Comparison between Merrifield–Simmons index and some vertex-degree-based topological indices. *Comput. Appl. Math.* **2023**, *42*, 89, <https://doi.org/10.1007/s40314-023-02240-x>.
27. Rajpoot, A.; Selvaganesh, L. Bounds of the Symmetric Division Deg Index for Trees and Unicyclic Graphs with a Perfect Matching. *Iranian J. Math. Chem.* **2020**, *11*, 141–159, <https://doi.org/10.22052/ijmc.2020.214829.1481>.
28. Rajpoot, A.; Selvaganesh, L. Study of Bounds and Extremal Graphs of Symmetric Division Degree Index for Bicyclic Graphs with Perfect Matching. *Iranian J. Math. Chem.* **2022**, *13*, 145–165, <https://doi.org/10.22052/ijmc.2022.243396.1605>.
29. Rajpoot, A.; Selvaganesh, L. Potential application of novel AL-indices as molecular descriptors. *J. Mol. Graph. Model.* **2023**, *118*, 108353, <https://doi.org/10.1016/j.jmglm.2022.108353>.
30. Rajpoot, A.; Selvaganesh, L. Bounds and extremal graphs of second reformulated Zagreb index for graphs with cyclomatic number at most three. *Kuwait J. Sci.* **2022**, *49*, <https://doi.org/10.48129/kjs.v49i1.10447>.
31. Das, K.C.; Mondal, S. On neighborhood inverse sum indeg index of molecular graphs with chemical significance. *Inf. Sci.* **2023**, *623*, 112–131, <https://doi.org/10.1016/j.ins.2022.12.016>.
32. Mondal, S.; De, N.; Pal, A. Neighborhood degree sum-based molecular descriptors of fractal and Cayley tree dendrimers. *Eur. Phys. J. Plus* **2021**, *136*, 303, <https://doi.org/10.1140/epjp/s13360-021-01292-4>.
33. Estrada, E. Characterization of 3D molecular structure. *Chem. Phys. Lett.* **2000**, *319*, 713–718, [https://doi.org/10.1016/S0009-2614\(00\)00158-5](https://doi.org/10.1016/S0009-2614(00)00158-5).

34. Hayat, S.; Imran, M.; Liu, J.-B. Correlation between the Estrada index and π -electronic energies for benzenoid hydrocarbons with applications to boron nanotubes. *Int. J. Quantum Chem.* **2019**, *119*, e26016, <https://doi.org/10.1002/qua.26016>.
35. Gutman, I. Some properties of the Wiener polynomial. *Graph Theory Notes N.Y.* **1993**, *125*, 13-18.
36. Hosoya, H. On some counting polynomials in chemistry. *Discret. Appl. Math.* **1988**, *19*, 239-257, [https://doi.org/10.1016/0166-218X\(88\)90017-0](https://doi.org/10.1016/0166-218X(88)90017-0).
37. Wiener, H. Structural Determination of Paraffin Boiling Points. *J. Am. Chem. Soc.* **1947**, *69*, 17-20, <https://doi.org/10.1021/ja01193a005>.
38. Hosoya, H. Topological index. Topological Index. A Newly Proposed Quantity Characterizing the Topological Nature of Structural Isomers of Saturated Hydrocarbons. *Bull. Chem. Soc. Jpn.* **1971**, *44*, 2332-2339, <http://dx.doi.org/10.1246/bcsj.44.2332>.
39. Klein, D.J.; Lukovits, I.; Gutman, I. On the Definition of the Hyper-Wiener Index for Cycle-Containing Structures. *J. Chem. Inf. Comput. Sci.* **1995**, *35*, 50-52, <https://doi.org/10.1021/ci00023a007>.
40. Deutsch, E.; Klavžar, S. M-polynomial and Degree-based Topological Indices. *Iranian J. Math. Chem.* **2015**, *6*, 93-102, <https://doi.org/10.22052/ijmc.2015.10106>.
41. Masmali, I.; Naeem, M.; Ishaq, M.; Koam, A.N.A. Estimation of the physiochemical characteristics of an antibiotic drug using M-polynomial indices. *Ain Shams Eng. J.* **2023**, *14*, 102539, <https://doi.org/10.1016/j.asej.2023.102539>.
42. Mondal, S.; Das, K.C. On the Sanskruti index of graphs. *J. Appl. Math. Comput.* **2023**, *69*, 1205-1219, <https://doi.org/10.1007/s12190-022-01789-w>.

Publisher's Note & Disclaimer

The statements, opinions, and data presented in this publication are solely those of the individual author(s) and contributor(s) and do not necessarily reflect the views of the publisher and/or the editor(s). The publisher and/or the editor(s) disclaim any responsibility for the accuracy, completeness, or reliability of the content. Neither the publisher nor the editor(s) assume any legal liability for any errors, omissions, or consequences arising from the use of the information presented in this publication. Furthermore, the publisher and/or the editor(s) disclaim any liability for any injury, damage, or loss to persons or property that may result from the use of any ideas, methods, instructions, or products mentioned in the content. Readers are encouraged to independently verify any information before relying on it, and the publisher assumes no responsibility for any consequences arising from the use of materials contained in this publication.